Stochastic resonance and hysteresis in climate with state-dependent fluctuations

Moupriya Das* and Holger Kantz†
Max Planck Institute for the Physics of Complex Systems, 01187 Dresden, Germany

(Received 4 March 2020; revised manuscript received 15 May 2020; accepted 8 June 2020; published 29 June 2020)

We consider two aspects in climatic science where bistability between the two stable states of the systems is observed. One is the transition between the glacial and the interglacial period in Earth's glacial cycle. Another is the thermohaline circulation in the North Atlantic ocean. Both of these phenomena can be modeled by the overdamped dynamics of a Brownian particle in a double-well potential subject to periodic forcing. For the former case, the two wells represent two different climates and the periodic forcing is sufficiently weak not to cause a transition between the two states without the effect of the noise. Whereas in case of the latter phenomenon, the two states correspond to the two different conditions of the flow and the strength of the periodic forcing is high enough to give rise to hysteresis in the system. We propose that one important component of the dynamics, short-term fluctuations related to weather, in both of these cases, depends on the current climatic state of the system. This leads to introduction of the state-dependent diffusion coefficients in the dynamics because the diffusion coefficient represents the strength of the fluctuations. We justify our argument by analyzing the δ^{18}O record for the glacial cycle model. We have shown that this consideration can produce certain features in the dynamics which agree with the real observations in case of both glacial cycles and thermohaline flow.

DOI: 10.1103/PhysRevE.101.062145

I. INTRODUCTION

In their seminal paper [1], Benzi *et al.* introduced the concept of stochastic resonance as a first example for the constructive role of noise in nonlinear systems. In order to explain the observed almost-periodicities in the glaciation of the Earth they considered the stochastic forcing of a particle in a double-well potential with periodic perturbations, where the latter are too weak to make the particle hop from one well to another. The noise amplitude can be translated into a timescale through the Kramers escape rate, proportional to $e^{-\Delta V/kT}$, where ΔV is the height of the potential barrier between the two minima and kT stands for the intensity of thermal fluctuations in terms of a diffusion constant. If this timescale is of the order of the period of the weak periodic driving, then there is a chance that the particle hops once per half period due to the noise and hence is in almost-synchrony with the periodic driver. Hänggi and Marchesoni and several others [2–8] have refined this argument, so that today this phenomenon is understood in great theoretical detail. Stochastic resonance has been observed in many different settings since then, among them are neuronal systems [9–11], environmental systems [12–14], and biochemical systems [15–17]. In several of these cited works it has been highlighted that stochastic resonance is a phenomenon where noise enhances a deterministic signal and thereby plays a constructive role. It is even thought to be an amplification mechanism for nerve sensing of signals of very small strength [18–20]. On the other hand, more-detailed analysis has raised doubts about the relevance of stochastic resonance for the system where it had been first proposed, the alternation in the glacial states of the Earth [21].

In view of References [21,22], we propose here a technically simple but conceptually relevant extension of the classical stochastic resonance model, namely state-dependent noise amplitude, sometimes also called multiplicative noise. For simplicity and in order to keep the number of free parameters small, the noise strength in our model will be constant within each well but different for the two wells. In the simple interpretation of the noise strength as the timescale for stochastic hopping from one well to the other, our generalization means that this timescale differs between the two potential wells. While the overall features of stochastic resonance remain unchanged, this additional freedom allows us to introduce asymmetry into the problem and to adapt the model better to properties of the system which one wants to design.

In the following, we will first introduce our generalized stochastic resonance model and show some of its features. We will then study two applications in detail, namely the well-known glacial-interglacial oscillations [1,2,8,23–25], and a model for oceanic circulation [26–28]. In the first case, our model is able to reproduce asymmetries between warm and cold periods which one observes in data, but moreover, by data analysis, we can verify independently the existence of different diffusion constants in the two potential wells. For

*Corresponding author: mdas@pks.mpg.de
†kantz@pks.mpg.de

the oceanic flow, we can reproduce asymmetries which have be previously found in more complex models.

II. THE SYSTEM AND THE DYNAMICS

The Langevin dynamics of an overdamped Brownian particle in a bistable potential subject to periodic forcing can be employed to understand the process of stochastic resonance to explain glacial cycles [1,2,8,23–25] and hysteresis in thermohaline circulation [26–28]. The equation of motion in dimensionless form can be written as

$$\dot{x} = -ax^3 + bx + A_0\sin(\omega t) + \sqrt{D}\xi(t), \tag{1}$$

where x is the dynamical variable and t represents time; a and b are constants and are characteristics of the potential; A_0 and ω are the amplitude and frequency of the periodic force, respectively; and $\xi(t)$ is the zero-mean, Gaussian, white noise. The strength of the noise is given by D which is dependent on the temperature of the system. The properties of $\xi(t)$ are given by

$$\begin{aligned}\langle\xi(t)\rangle &= 0,\\ \langle\xi(t)\xi(t')\rangle &= 2\delta(t-t').\end{aligned} \tag{2}$$

In absence of any external force, the positions of the minima are at $\pm\sqrt{\frac{b}{a}}$ and the depth of the potential is given by $\frac{b^2}{4a}$. When the forcing amplitude is not too large, the positions of the minima and the barrier height of the potential do not change significantly. Consequently, the two minima of the potential correspond to the two states of the system. More accurately, it can be said that the two wells of the potential represent the two states at any instant of time and the states are quantified by the positions near the minima in the asymptotic limit.

For the stochastic resonance model of glaciation, the dynamical variable x is related to the Earth's global mean temperature [1], and for the model corresponding to the Atlantic thermohaline flow x represents North Atlantic Deep Water (NADW) circulation [27]. The two minima of the bistable potential represent two steady-state temperatures for the stochastic resonance climate model and two steady-state flows for the thermohaline circulation model. The weather-dependent fluctuations are incorporated in the dynamics through the noise term. In the theoretical studies on these phenomena, it has been considered so far that the strength of the fluctuations coming from the surroundings is the same for both the states. Here, we argue that the environmental fluctuations will be affected by the current state of the system. For example, we consider that in case of the climate change model, the weather-dependent fluctuations will be different for the low-temperature and the high-temperature phases. The justification for this argument is that the fluctuations appear from the short-term weather change which is directly affected by temperature. Similarly, it is considered that the fluctuations in the thermohaline circulation depend on the state of the NADW circulation to incorporate the environmental effect. Therefore, the overdamped Langevin dynamics [Eq. (1)] can be modified as

$$\dot{x} = -ax^3 + bx + A_0\sin(\omega t) + \sqrt{D(x)}\xi(t), \tag{3}$$

where $D(x)$ is the state-dependent strength of the fluctuations. We assume that $D(x) = D_1$ for the left potential well and $D(x) = D_2$ for the right potential well, for simplicity.

III. RESULTS AND DISCUSSIONS

A. Synchronization of the periodic forcing and the response of the system

During stochastic resonance, the periodic drive and the response of the system become synchronized to produce amplification of weak periodic forcing in presence of noise. We try to understand in detail this process of synchronization in system with state-dependent fluctuations. Therefore, before going into the discussion of the two models related to the climate science, we present the results from our systematic study to understand the course of synchronization of the external periodic forcing and the feedback of the system with state-dependent fluctuations. We compare our results with classical stochastic resonance case.

To measure the extent of synchronization, we consider the Fourier quantifier which is well known in the study of stochastic resonance [29]. We estimate the cosine and sine components (A_c and A_s, respectively,) of the response function, i.e., $x(t)$'s time series over a number of periods. The components A_c and A_s can be represented as follows:

$$\begin{aligned}A_c &= \frac{1}{nT}\int_0^{nT} x(t)\cos(\omega t)dt,\\ A_s &= \frac{1}{nT}\int_0^{nT} x(t)\sin(\omega t)dt,\end{aligned} \tag{4}$$

where $T = 2\pi/\omega$ is the time period of the periodic forcing and n is the number of periods. The response amplitude or the Fourier quantifier Q has the form

$$Q = \sqrt{A_c^2 + A_s^2}. \tag{5}$$

To calculate Q in terms of A_c and A_s, we solve $x(t)$ considering the Langevin dynamics Eq. (3). We have used improved Euler algorithm or Heun's method which is essentially a second order Runge-Kutta method [30] to solve the dynamics [Eq. (3)]. The noise term has been generated using Box-Muller algorithm. The time step has been taken to be equal to 10^{-3}. We have considered the parameter set used in a previous study regarding stochastic resonance [5] to compare our results with the classical case. The values of a and b are taken to be equal to 1. The amplitude of the periodic drive A_0 is considered to be equal to 0.2 and its frequency ω has been kept constant at 0.01. We have considered 1000 cycles to calculate Q and the quantifier has also been averaged over 100 trajectories.

The general idea to visualize stochastic resonance using the quantifier Q is to estimate the measure by varying the noise strength D and find its maxima as a function of D. In resonance condition, the periodic forcing and the response of the system are synchronized to the maximum extent. The greater is the degree of synchronization, the larger is the value of Q. Therefore, Q exhibits a maximum at a value of D which corresponds to the resonance situation. For the above-mentioned parameter set, the resonance is observed close to

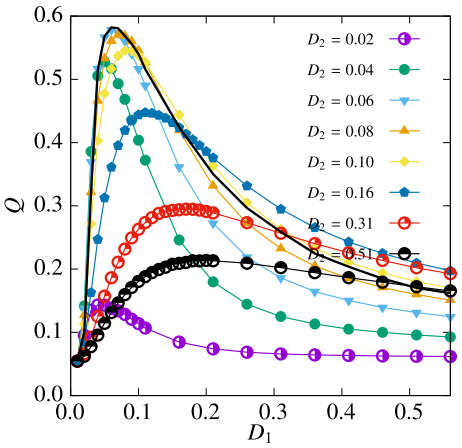

FIG. 1. Representative variations of Q versus D_1 for several values of D_2. The values of a and b are 1. The amplitude of the periodic forcing A_0 is 0.2 and the corresponding frequency ω is 0.01. The solid black line represents the curve obtained for classical stochastic resonance case.

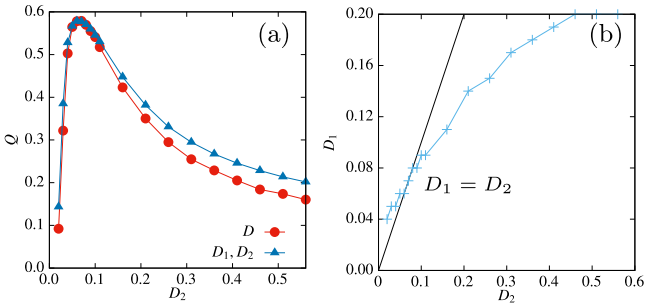

FIG. 2. (a) Comparison of the variation of the Q versus noise strength of one of the well (here right well) for the system with state-dependent diffusion coefficient with the classical stochastic resonance case. The parameter set is the following: $a = b = 1$, $A_0 = 0.2$, and $\omega = 0.01$. (b) D_1 as a function of D_2 corresponding to the maximum of the Q versus D_1 plot for several values of D_2 for the same parameter set. The black line represents the $D_1 = D_2$ condition.

$D = 0.06$ [5]. We keep the diffusion coefficient of the right potential well, i.e., D_2 fixed and vary the diffusion coefficient of the left potential well, i.e., D_1 to calculate Q. We vary D_1 starting from 0.02 to 0.56 and calculate Q for several values of D_2 ranging between 0.02 and 0.56. We have illustrated the variations of Q as a function of D_1 for some representative values of D_2 in Fig. 1. In our case, we have two noise parameters D_1 and D_2. Our study shows that for different values of D_2, we get maximum of Q corresponding to different values of D_1 and the numerical values of Q representing the maxima also vary depending on the combination of D_1 and D_2. The easiest way to quantitatively compare the present scenario with the classical stochastic resonance case is to join the maximum of the Q versus D_1 curve for several values D_2 and correlate it with the typical variation of Q against D for the standard case. However, for the present study, the maximum of Q is a function of two independent variables D_1 and D_2. We observe that the highest maximum appears in the Q versus D_1 curve for $D_2 = 0.06$ and the corresponding D_1 value is also 0.06. This result agrees with the classical stochastic resonance case where one observes maximum of Q at $D = 0.06$. We note that near the peak of the Q versus D_1 curve, the maximum of Q occurs when $D_1 = D_2$, suggesting the fact that synchronization is most effective when the diffusion timescales of the two wells are equal. The numerical values of Q in the curve which has been obtained by linking the maxima of the Q versus D_1 curve for different values of D_2 are same as that in the classical curve close to the peak. However, the two curves deviate away from the peak. We have presented this result in Fig. 2(a). We also detect that the maximum in the Q versus D_1 curve emerges for the condition $D_1 \neq D_2$ when one is away from the peak [Fig. 2(b)] and the value of Q is higher for the present scenario as compared to the classical stochastic resonance case. This result suggests that when one is away from the resonance condition, i.e., when synchronization is not so effective, a difference in the value of noise strength in different wells can act to bring better synchrony in the periodic signal and the response of the system. This points toward a subtle difference in the characteristic of our study with the conventional stochastic resonance case.

B. Glaciation stages

The concept of stochastic resonance was first introduced to interpret the recurrent occurrence of glacial and interglacial periods [1,23,24]. The double-well potential represents Earth's climate. The two minima of the double-well potential represent two stable temperatures; one corresponds to the glacial and the other to the interglacial climate. There occurs very small periodic modulation of the Earth's orbital eccentricity which is represented by the weak periodic perturbation. Annual fluctuations of solar radiation can be considered as the short-term environmental fluctuations and it is modeled by the zero-mean, Gaussian white noise. Equation (1) can represent this dynamics. In the standard model, the dimensionless constants a and b have values equal to 1 which gives potential minima at $x_m = \pm 1$, the amplitude of the periodic forcing A_0 is 0.11, and the frequency of modulation ω is considered to be $2\pi/6000$ and the value of D is varied between 0.01 to 0.3 [24].

In our model, we consider that the short-term fluctuations in solar radiation affects the glacial and the interglacial climate differently. Physically, it can be explained like this. The cloud coverage over the Earth controls the amount of solar radiation entering the Earth's atmosphere and also the reflection of the ultraviolet radiation outside, not entering the system. The extent of cloud coverage over the Earth is supposed to be different for two different climates, the glacial and the interglacial climates. Therefore, effectively the solar radiation fluctuations affect these two different climates with different strength. So, we argue that the strength of the noise or the diffusion coefficient associated with the two climatic states would be different.

For the system considered, the potential minima are at ± 1 in absence of any external bias. Let us consider that the dynamical variable at the potential minimum which is $x_m = 1$ corresponds to the interglacial climate and that at the $x_m = -1$ represents the glacial atmosphere. Due to the effect of the weak periodic forcing and noise, transitions take place between the two wells of the bistable potential, i.e., between

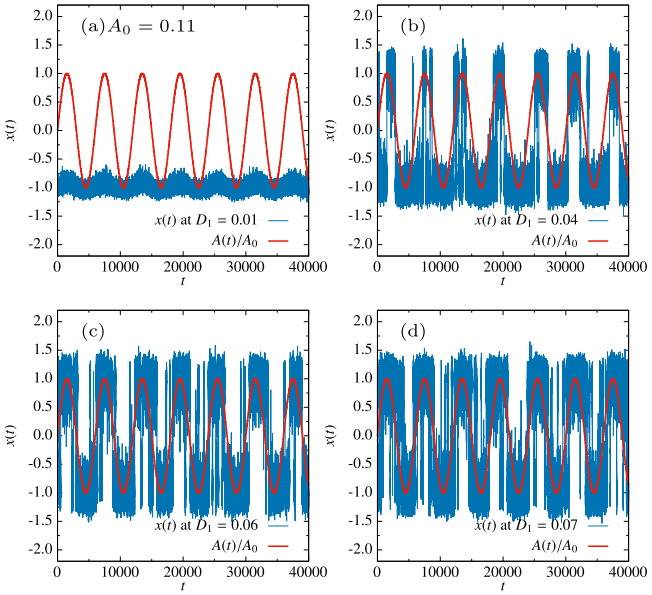

FIG. 3. Time series of the dynamical variable $x(t)$ (noisy lines) along with the periodic forcing $A(t)$ (smooth lines) for four different values of D_1 at (a) 0.01, (b) 0.04, (c) 0.06, and (d) 0.07. The value of D_2 has been kept constant at 0.07. a and b have been taken to be equal to 1. A_0 is 0.11 and ω has value equal to $2\pi/6000$.

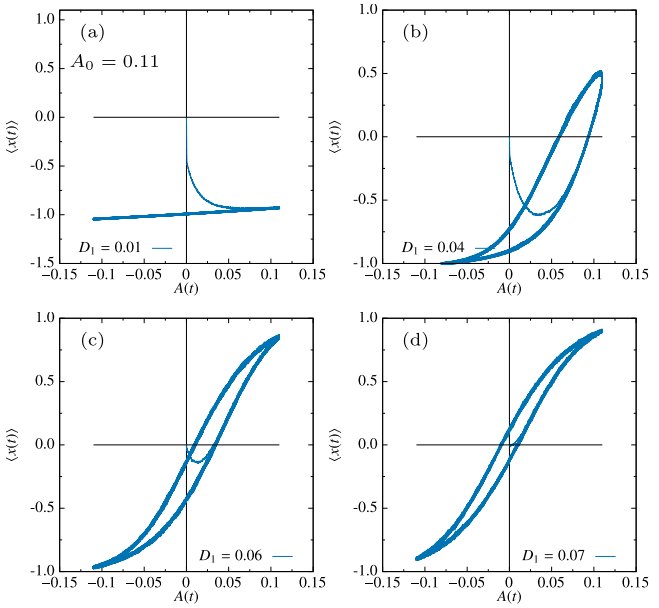

FIG. 4. Hysteresis curves, $\langle x(t) \rangle$ versus $A(t)$, for four different values of D_1 at (a) 0.01, (b) 0.04, (c) 0.06, and (d) 0.07. The value of D_2 has been kept constant at 0.07. a and b have been taken to be equal to 1. A_0 is 0.11 and ω has value equal to $2\pi/6000$.

the two different climates. We have used the same method as described in the previous subsection to solve the Langevin dynamics [Eq. (3)] and to generate the noise term with the same time step value equal to 10^{-3}. To establish our case, we proceed with Eq. (3) and simulate the dynamics with the same parameter set as described in Ref. [24] but with two different diffusion coefficients corresponding to the two wells. We have kept the diffusion coefficient of the right well D_2 to be fixed at 0.07 and varied D_1 starting from 0.01. In Fig. 3 we have represented the time series of the periodic signal and the dynamical variable $x(t)$ for four different values of D_1 at 0.01, 0.04, 0.06, and 0.07. The time series of $x(t)$ at the lowest value of D_1, i.e., at 0.01 [Fig. 3(a)] suggests that there occurs no transition between the climatic states if the noise strength is too small. The transitions take place if D_1 is increased. This is observed in Figs. 3(b)–3(d). The interesting point to note here is that the residence time at the two states are different if the values of the respective diffusion coefficients D_1 and D_2 are different. For example, at $D_1 = 0.04$ and $D_1 = 0.06$ (which are less than $D_2 = 0.07$), the dynamical variable spends more time at the glacial state, whereas at $D_1 = 0.07$ (which is equal to the value of D_2) the residence time at both the states; i.e., at the glacial and at the interglacial climate, is the same. This is an important observation because our consideration of different strength of short-term climate fluctuations corresponding to two different states, supports the asymmetric nature of the glacial cycles [22] and also the fact that the glacial periods are in general longer than the interglacial periods [31]. The numerical results obtained from our model suggest that assigning lower level of weather related fluctuations to the glacial period makes the climate to stay at this state for a longer span of time as compared to the interglacial period.

The response of the system, $x(t)$, does not show hysteretic behavior with respect to the periodic perturbation for a single trajectory. However, interestingly, the average value $\langle x(t) \rangle$ forms hysteresis loops when plotted against the periodic driving $A(t)$. This has been shown in Figs. 4(a)–4(d) for four different values of D_1 at $D_2 = 0.07$. Here we have presented the results obtained by averaging over 10^6 number of trajectories. The same can be obtained by taking long-time average of the $x(t)$ time series. The hysteresis cycles are asymmetric around the origin if the values of the noise strength associated with the two wells are different. So, for D_1 less than D_2, we get asymmetric hysteresis loops [Figs. 4(a)–4(c)] and the equal value of D_1 and D_2 gives rise to symmetric hysteresis loop [Fig. 4(d)].

To assess our argument by analyzing the real data, we consider benthic δ^{18}O record proposed by Lisiecki *et al.* [32]. The data have been presented in Figs. 5(a) and 5(b). The curves represent composite deep sea foraminiferal isotope

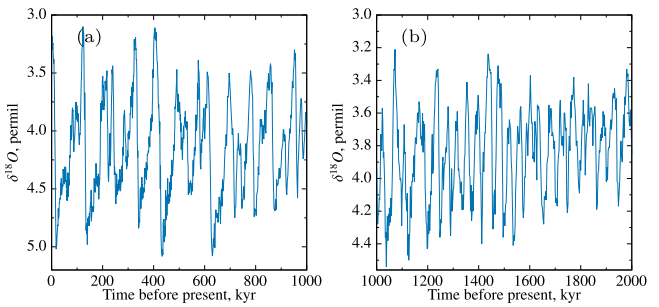

FIG. 5. Composite deep sea foraminiferal isotope record (Lisiecki and Raymo 2005 [32]) for (a) 0 to 1000 kyr before present time and (b) 1000 to 2000 kyr before present time.

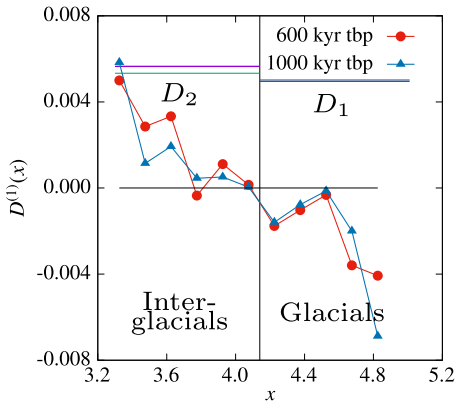

FIG. 6. Variation of the state-dependent drift $D^{(1)}(x)$ with respect to x for the δ^{18}O record (Lisiecki and Raymo 2005 [32] considering up to 600 and 1000 kyr before present time). The two states, glacials and interglacials, and their corresponding diffusion coefficients D_1 and D_2 have also been indicated. The thick lines indicate the values of D_1 and D_2 for the time span of 600 kyr before present time and the thin lines represent the same when we consider up to 1000 kyr before present time.

record [22,32]. The middle Pleistocene transition is seen around 1 million years before the present time. The characteristics of the cycles up to 1000 kyr before present time are different from earlier cycles (1000 to 2000 kyr before present time). The former cycles are asymmetric [Fig. 5(a)] and the latter are symmetric [Fig. 5(b)]. We concentrate on the asymmetric cycles which correspond to the slow cooling from the interglacials to glacials and fast warming from the glacials to interglacials [22]. The related model temperature anomaly data qualitatively follow the same structure as that of the δ^{18}O record as shown in Figs. 5(a) and 5(b) [22]. We take an average of the data and consider that there exist two states, one below the average value and the other above the average value. One of the states corresponds to the glacials and the other to the interglacials. For the δ^{18}O data, the values below the average represent interglacial climate and that above the average correspond to glacial period. We calculate the state-dependent drift $D^{(1)}(x)$ [33–37] following the equation

$$D^{(1)}(x) = \lim_{\Delta\to 0} \frac{1}{\Delta} \langle x_{t+\Delta} - x_t \rangle_x. \tag{6}$$

where the average $\langle \ldots \rangle_x$ represents the conditional average that $x_t = x$. $D^{(1)}(x)$ represents the deterministic force, i.e., the negative gradient of the potential [38]. Here we can expect the dependence of $D^{(1)}(x)$ with respect to x to be like $x - x^3$ as the underlying potential is supposed to possess bistability. We have presented the result of our analysis in Fig. 6. Probably, due to the limitation on the availability of the data, we are unable to see the clear trend of the cubic function in the calculated force arising from the bistability of the potential. Still we observe that the drift $D^{(1)}(x)$ is a decaying function of x which has a metastable point very close to the average value of x. Therefore, we consider the two states to lie below and above the average value of x. We present the variation of $D^{(1)}(x)$ with respect to x considering the data up to 600 and 1000 kyr before present time. Both of the curves show similar behavior. We measure the state-dependent diffusion coefficients [33–37] corresponding to these two states, i.e., the two climates following the equation

$$D(x) = \lim_{\Delta\to 0} \frac{1}{2\Delta} \langle (x_{t+\Delta} - x_t)^2 \rangle_x. \tag{7}$$

Here also the average $\langle \ldots \rangle_x$ measures the conditional average that $x_t = x$. The calculations show that the diffusion coefficient corresponding to the interglacial period is higher as compared to the glacial period. If we consider up to 600 kyr before present time, then the effective diffusion coefficients are 4.965×10^{-3} and 5.648×10^{-3} for the glacials and interglacials, respectively. When we take into account time up to 1000 kyr before present time the values of D_1 and D_2 become 5.023×10^{-3} and 5.334×10^{-3}, respectively. The errors in the values of D_1 and D_2 are of the order of 10^{-5} in all cases. These effective diffusion coefficients have been presented in Fig. 6 by D_1 and D_2. Although up to 1000 kyr before present time the cycles show similar behavior, we suggest that it is relevant to calculate the drift and diffusion coefficients of the time series for 600 kyr before the present time because within this time segment successive data are available for the smallest time interval [32]. Therefore, this time duration provides a greater number of data at hand for a given time span and a better statistics. We also see that the difference in values of D_1 and D_2 is more significant when we consider up to 600 kyr before the present time. As the temperature anomaly data follow the same structure as that of the δ^{18}O data, one can expect the diffusion coefficients corresponding to the temperature data to behave in a similar way, i.e., the diffusion coefficient representing the interglacial climate would be higher as compared to that corresponding to the glacial atmosphere. This is what we have considered while simulating our model [Eq. (3)] and observed that the glacials last longer than the interglacials. The evaluation of the two different diffusion coefficients corresponding to the two different climatic states from the real data supports our argument. The analysis of our model shows that the consideration of different strength of short-term weather fluctuations, i.e., the diffusion coefficients of the two climatic states can explain different duration of glacials and interglacials.

C. Thermohaline circulation

Bistability in climatic science is also observed in the case of North Atlantic thermohaline circulation [26–28]. The present-day Gulf Stream carries a large amount of heat from the tropical region to the very north of the Atlantic ocean. This heat transport occurs due to the vertical reversing of the cell linked to the NADW formation [26]. Warmer surface water flows to the northand then goes down the surface and circulates toward the south as cold deep water. This is the reason for the milder climate in Western Europe (northern North Atlantic) compared to the regions in the Pacific of the same latitude. However, there is another stable state for the thermohaline circulation which transports a lesser amount of heat to the north. It is considered that in the past the thermohaline flow was confined to that state [26,28].

The observed bistability suggests that NADW circulation is a nonlinear system and the model studies have shown that the system exhibits hysteresis behavior between the two states

if the freshwater forcing exceeds a certain value [26,39–43]. The model proposed by H. Stommel, which is known as Stommel's box model [39], explains the bistability in NADW circulation. In that model, the ocean at the low latitude and at the high latitude are represented by two different boxes and two different values of temperature and salinity are assigned to these boxes. The dynamics of the temperature difference and the salinity difference between the two regions can be modeled in different ways [44] and their dynamics is coupled through the density difference [28]. Taking into account of the fact that the coupled dynamics represents a slow-fast system, the two-dimensional dynamics can be reduced to the form of Eq. (1) [28]. Here the dynamical variable x represents a quantity that signifies NADW circulation, the periodic forcing term $A_0\sin(\omega t)$ is proportional to the freshwater circulation which is affected by the imbalances between the evaporation prevailing at the low amplitudes and precipitation dominating at the high amplitudes. The noise term $\sqrt{D}\xi(t)$ represents weather-dependent fluctuations.

Here also we consider that the weather-dependent fluctuations which arise as a consequence of the variation of evaporation and precipitation affect the two stable states of the system, i.e., the two different conditions of the NADW flow, differently. Different situations of the NADW flow influence the change in weather, for example, the temperature of the atmosphere directly. These distinct weathers control the process of evaporation and precipitation in their particular way. Consequently, the fluctuations coming from the weather depend on the current state of the weather itself. Therefore, one can expect the short-term weather fluctuations to regulate the two states of the NADW flow in different manner. So we assign two different values of the noise strength or diffusion coefficient corresponding to the two wells and solve the dynamics [Eq. (3)]. We consider that a and b have values equal to 1 and A_0 is 0.4, an amplitude value of the periodic forcing that is high enough to cause hysteresis. We consider D_2 to be fixed at 0.07 and change D_1 starting from 0.01 to 0.07. The time series of $x(t)$ along with the periodic forcing $A(t)$ has been presented in Figs. 7(a)–7(d) for these four D_1 values at $D_2 = 0.07$ and $\omega = 0.005$. The observations suggest that there is delay in response of the system with respect to the periodic forcing which ultimately gives rise to hysteresis and the delay is more prominent when the difference of the values of D_1 and D_2 is more. To understand the effect of the hysteresis better, we take an average over 10^6 number of trajectories. This can also be thought as a long time average of $x(t)$ and considered to represent the equilibrium feature of the dynamics. The results have been shown in Figs. 8(a)–8(d) for the same parameter set as in Figs. 7(a)–7(d) with three different ω values of 0.001, 0.005, and 0.01. $\langle x(t)\rangle$ has been plotted against $-A(t)$ to match the directionality in previous studies [26,27]. It is observed that the consideration of the different values of D_1 and D_2 produces hysteresis loops which are asymmetric around the origin [Figs. 8(a)–8(c)] and the curves are symmetric for the equal values of D_1 and D_2 [Fig. 8(d)]. This is consistent with the previous observations in model experiments [26] and the features of the hysteresis loops studied with different theoretical models [27] which are much more complex and have higher dimensionality than that of our current model. These earlier investigations also suggest that the right branch of the hysteresis loop is rounded. This is expected because of

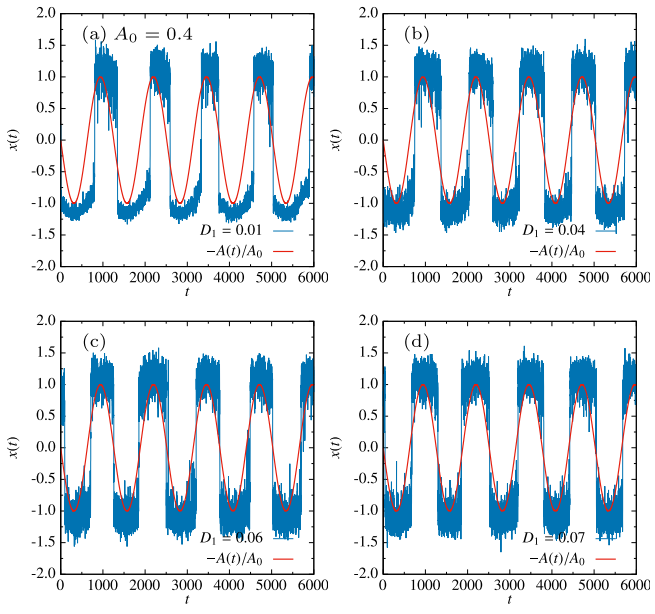

FIG. 7. Time series of the dynamical variable $x(t)$ (noisy lines) along with the periodic forcing $A(t)$ (smooth lines)for four different values of D_1 at (a) 0.01, (b) 0.04, (c) 0.06, and (d) 0.07. The value of D_2 has been kept constant at 0.07. a and b have been taken to be equal to 1. A_0 is 0.4 and ω has value equal to 0.005.

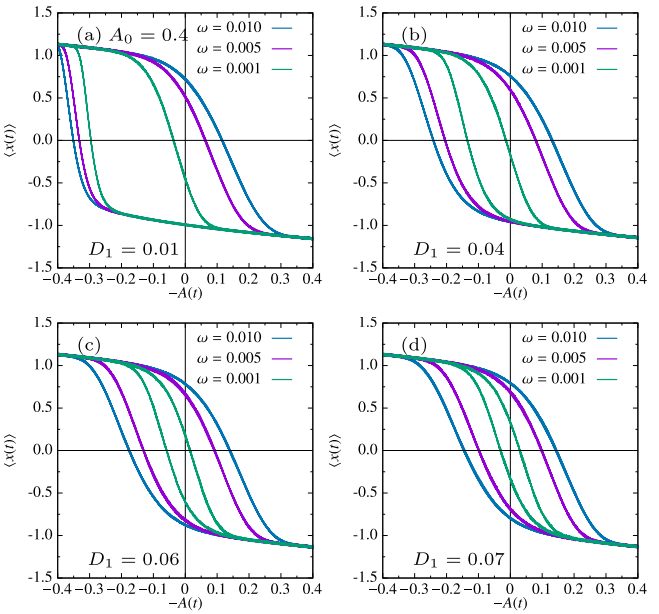

FIG. 8. Hysteresis curves, $\langle x(t)\rangle$ versus $A(t)$, for four different values of D_1 at (a) 0.01, (b) 0.04, (c) 0.06, and (d) 0.07. The value of D_2 has been kept constant at 0.07. a and b have been taken to be equal to 1. A_0 is 0.4. For each D_1 value three different ω values (0.001, 0.005, and 0.01) have been considered. The loop area increases with increasing ω. So we get the smallest hysteresis loop at $\omega = 0.001$ and the hysteresis loop has the maximum size at $\omega = 0.01$.

the existence of the underlying parabolic equilibrium curve that is obtained from the Stommel's model [26,27]. This characteristic feature is reflected in the hysteresis loops when D_1 and D_2 are much different [Fig. 8(a)]. It was observed before that with increasing periodic forcing, the right half of the hysteresis loops shifts toward the left [26]. Our model study also supports this fact. The point to be mentioned here is that we have arbitrarily assigned lower and higher values to D_1 and D_2, respectively. Nonetheless, the consideration of the reverse will not change the argument about the asymmetric nature and the other characteristics of the observed hysteresis loops. The important aspect to note here is that to explain the hysteresis phenomenon in thermohaline circulation many models of high to intermediate complexity have been introduced [27]. However, despite the simplicity of the current one-dimensional model representing NADW circulation, we can capture the features of the hysteresis behavior exhibited by the system when we consider that the short-term weather related fluctuations depend on the current state of the system.

IV. CONCLUSION

We consider two phenomena in climate science where bistability between two states is observed. One is the transition between the two climatic states, the glacial and the interglacial periods. Here these two states can be represented by the two minima of a double-well potential. Another one is the thermohaline circulation in North Atlantic ocean where two different conditions of the NADW flow are considered to form the two states of the system. This system can also be modeled with a bistable potential, the two wells signifying two different types of the flow. In both cases, the dynamics are subject to a periodic forcing. For the climate change model the periodic forcing is connected to the change of Earth's orbital eccentricity and is very weak in nature. On the other hand, the periodic perturbation in NADW circulation has large amplitude to cause hysteresis in the system and it is equivalent to the freshwater flux. The other important factor that controls the dynamics is the short-term weather-dependent fluctuations. This is represented by Gaussian, white noise in the dynamics. The strength of the noise dictates the extent of fluctuations and is a measure of the diffusion coefficient.

We take into account the Langevin dynamics of an overdamped Brownian particle in a bistable potential, subject to periodic forcing to represent the two systems. This is the simplest model that can capture the essential dynamics. In all of the previous studies, it has been considered that the short-term weather-dependent fluctuations affect the two states in a similar way. Here in this paper, we argue that there is reason to assume that the effect of the fluctuations on the two states of the systems is different as the fluctuations bear the characteristics of the corresponding state. This hypothesis makes the diffusion coefficient state dependent. Introduction of the idea of the different diffusion coefficients corresponding to the two different states helps to reproduce important features of the dynamics with the help of the simple bistable model. For the climate change model, consideration of the lower diffusion coefficient associated with the state of the glacial period makes the system to stay for longer time at the glacials compared to the interglacials. We justify this assumption by analyzing δ^{18}O records obtained in previous observation. This investigation shows that the diffusion coefficients calculated from the real data are also different for the two states and it has smaller value for the state corresponding to the glacial for the first one million year. The observation of the longer duration of the glacial period as compared to the interglacial period in our simulation study is in agreement with what one views in Earth's glacial cycle. In thermohaline circulation model, assignment of varied strength of weather-dependent fluctuations produces asymmetric hysteresis loops which were also observed in previous model experiments and theoretical studies. Therefore, we propose that the consideration of the state-dependent diffusion coefficients is important in these two climate models because this assumption can generate some actual features of the dynamics when incorporated in the standard model.

[1] R. Benzi, A. Sutera, and A. Vulpiani, J. Phys. A: Math. Gen. **14**, L453 (1981).

[2] L. Gammaitoni, P. Hänggi, P. Jung, and F. Marchesoni, Rev. Mod. Phys. **70**, 223 (1998).

[3] L. Gammaitoni, P. Hänggi, P. Jung, and F. Marchesoni, Eur. Phys. J. B **69**, 1 (2009).

[4] L. Gammaitoni, F. Marchesoni, E. Menichella-Saetta, and S. Santucci, Phys. Rev. Lett. **62**, 349 (1989).

[5] P. Jung and P. Hänggi, Phys. Rev. A **44**, 8032 (1991).

[6] L. Gammaitoni, F. Marchesoni, and S. Santucci, Phys. Rev. Lett. **74**, 1052 (1995).

[7] L. Gammaitoni, M. Löcher, A. Bulsara, P. Hänggi, J. Neff, K. Wiesenfeld, W. Ditto, and M. E. Inchiosa, Phys. Rev. Lett. **82**, 4574 (1999).

[8] A. R. Bulsara and L. Gammaitoni, Phys. Today **49**(3), 39 (1996).

[9] A. Longtin, J. Stat. Phys. **70**, 309 (1993).

[10] D. Nozaki, D. J. Mar, P. Grigg, and J. J. Collins, Phys. Rev. Lett. **82**, 2402 (1999).

[11] D. R. Chialvo, O. Calvo, D. L. Gonzalez, O. Piro, and G. V. Savino, Phys. Rev. E **65**, 050902(R) (2002).

[12] L. Stone, P. I. Saparin, A. Huppert, and Colin Price, Geophys. Res. Lett. **25**, 175 (1998).

[13] R. B. Alley, S. Anandakrishnan, and P. Jung, Paleoceanogr. Paleoclimatol. **16**, 190 (2001).

[14] S. De Martino, M. Falanga, and L. Mona, Phys. Rev. Lett. **89**, 128501 (2002).

[15] H. Qian and M. Qian, Phys. Rev. Lett. **84**, 2271 (2000).

[16] Z. Hou and H. Xin, J. Chem. Phys. **119**, 11508 (2003).

[17] K. Sriram and M. S. Gopinathan, Theor. Chem. Acc. **114**, 46 (2005).

[18] S. G. Lee and S. Kim, Phys. Rev. E **60**, 826 (1999).

[19] R. K. Adair, Proc. Natl. Acad. Sci. USA **98**, 7253 (2001).

[20] Stefan Martignoli, F. Gomez, and Ruedi Stoop, Sci. Rep. **3**, 2676 (2013).

[21] P. D. Ditlevsen, Paleoceanogr. Paleoclimatol. **24**, PA3204 (2009).

[22] I. Daruka and P. D. Ditlevsen, Clim. Dyn. **46**, 29 (2016).

[23] R. Benzi, G. Parisi, A. Sutera, and A. Vulpiani, Tellus **34**, 10 (1982).
[24] R. Benzi, A. Sutera, G. Parisi, and A. Vulpiani, SIAM (Soc. Ind. Appl. Math.) J. Appl. Math. **43**, 565 (1983).
[25] B. McNamara and K. Wiesenfeld, Phys. Rev. A **39**, 4854 (1989).
[26] S. Rahmstorf, Nature **378**, 145 (1995).
[27] S. Rahmstorf, M. Crucifix, A. Ganopolski, H. Goosse, Igor Kamenkovich, R. Knutti, G. Lohmann, R. Marsh, L. A. Mysak, Z. Wang, and A. J. Weaver, Geophys. Res. Lett. **32**, L23605 (2005).
[28] N. Berglund and B. Gentz, Stoch. Dynam. **02**, 327 (2002).
[29] M. Borromeo, G. Costantini, and F. Marchesoni, Phys. Rev. Lett. **82**, 2820 (1999).
[30] R. W. Hamming, *Numerical Methods for Scientists and Engineers* (McGraw–Hill, New York, 1973).
[31] J. M. K. C. Donev *et al.*, Energy education—Glacial and interglacial periods [online] (2018), https://energyeducation.ca/encyclopedia/Glacial_and_interglacial_periods.
[32] L. Lisiecki and M. E. Raymo, Paleoceanogr. Paleoclimatol. **20**, PA1003 (2005).
[33] S. Siegert, R. Friedrich, and J. Peinke, Phys. Lett. A **243**, 275 (1998).
[34] R. Friedrich and J. Peinke, Phys. Rev. Lett. **78**, 863 (1997).
[35] S. Luck, J. Peinke, and R. Friedrich, Phys. Rev. Lett. **83**, 5495 (1999).
[36] R. Friedrich, J. Peinke, and Ch. Renner, Phys. Rev. Lett. **84**, 5224 (2000).
[37] M. Ragwitz and H. Kantz, Phys. Rev. Lett. **87**, 254501 (2001).
[38] H. Risken, *The Fokker-Planck Equation* (Springer-Verlag, Berlin, 1984).
[39] H. Stommel, Tellus **13**, 224 (1961).
[40] F. Bryan, Nature **323**, 301 (1986).
[41] S. Manabe and R. J. Stouffer, J. Clim. **1**, 841 (1988).
[42] J. Marotzke and J. Willebrand, J. Phys. Oceanogr. **21**, 1372 (1991).
[43] U. Mikolajewicz and E. Maier-Reimer, J. Geophys. Res. **99**, 22633 (1994).
[44] P. Cessi, J. Phys. Oceanogr. **24**, 1911 (1994).